

Antisymmetric Raman response

Mattia Udina^{1,2} and Indranil Paul¹

¹Laboratoire Matériaux et Phénomènes Quantiques,
Université Paris Cité, CNRS, 75205 Paris, France

²Institut de Physique et Chimie des Matériaux de Strasbourg (UMR 7504),
Université de Strasbourg and CNRS, Strasbourg, 67200, France

(Dated: July 11, 2025)

We develop the theory of antisymmetric Raman response, defined as the difference between the Raman signals of two scattering geometries related by an exchange of mutually perpendicular incoming and the outgoing photon polarizations. Such responses, finite in orthorhombic or lower symmetry systems, are related to cross-susceptibilities of two Raman operators and are characterized by the absence of intraband terms. This is in contrast to standard Raman responses which measure auto-susceptibilities where both intra- and interband processes contribute. We illustrate the theory with examples from the charge density wave rare-earth tritellurides and the excitonic insulator Ta₂NiSe₅. Our theory establishes antisymmetric Raman response as a unique tool to probe microscopic features such as interband energy scales and to detect reflection symmetry breaking.

Introduction.— Inelastic light scattering, with distinct incoming and outgoing photons, or Raman response is an important tool to probe quantum materials [1–11]. The versatility of this technique stems from the ability to control the photon polarizations. In conventional usage, Raman response measures the auto-susceptibility of a second rank tensor operator $\hat{\Gamma}$, whose precise tensorial structure is determined by the aforesaid polarizations.

In this work we describe a new application of Raman scattering that probes the *cross-susceptibility* of two Raman operators $\hat{\Gamma}_1$ and $\hat{\Gamma}_2$. It is realized by comparing the signal I_{x_θ, y_θ} with mutually perpendicular in, out polarizations (x_θ, y_θ) , respectively, with I_{y_θ, x_θ} having the polarizations exchanged, see Fig. 1(a). We define $I_A(\Omega, \theta) \equiv I_{x_\theta, y_\theta}(\Omega) - I_{y_\theta, x_\theta}(\Omega)$ as *antisymmetric Raman response*. They are non-zero in orthorhombic or lower symmetry systems, as discussed below.

Our motivation is a recent experiment on the rare-earth tritellurides, where a noticeable antisymmetric Raman signal was detected in the charge density wave (CDW) phase [12]. The theory framework to explain it within the ambit of nonresonant scattering is currently missing, and our first goal is to develop it. As shown below, antisymmetric responses are considerably different from conventional Raman responses. Thus, our second goal is to establish antisymmetric Raman response as a complementary tool to probe electronic systems.

The following are our main results. (i) We connect $I_A(\Omega, \theta)$ to finite frequency cross-susceptibilities of two Raman operators by a fluctuation-dissipation relation. (ii) We show that the cross-susceptibilities have spectroscopic “gaps” due to the absence of intraband terms. (iii) We show that the frequency integrated cross-susceptibilities are thermodynamic order parameters for reflection symmetry breaking. (iv) We obtain a reciprocity relation that $I_A(\Omega, \theta)$ is an even function of an external magnetic field. (v) Using examples motivated by the tritellurides [12–19] and the exciton insulator

Ta₂NiSe₅ [20–23], we show that antisymmetric Raman response contain information that cannot be accessed using standard Raman response.

Formulation.— We start from the standard description of nonresonant Raman response. Ignoring geometric pre-

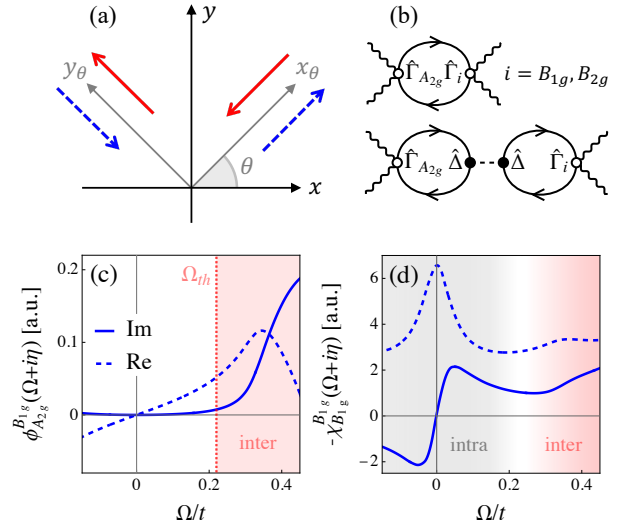


FIG. 1. (Color Online) (a) Raman intensity $I_{x_\theta, y_\theta}(\Omega)$ with mutually perpendicular in, out photon polarizations (red arrows). $I_{y_\theta, x_\theta}(\Omega)$ has polarizations exchanged (blue arrows). (b) Graphs of antisymmetric Raman responses from electrons (one loop) and a collective mode (two loop). $\hat{\Gamma}$ are Raman operators (white bullets), $\hat{\Delta}$ is electron (solid line) - collective mode (dashed line) coupling (black bullets). Comparing $\phi_{A_{2g}}^{B_{1g}}$ in (c) with $\chi_{B_{1g}}^{B_{1g}}$ in (d) for an orthorhombic metal. In (c) the imaginary and real parts are even and odd in Ω , respectively. In (d) it is opposite. Grey, red shades are intra- and interband dominated, respectively. $\text{Im}\phi_{A_{2g}}^{B_{1g}}(\Omega)$, lacking intraband component, is zero below threshold Ω_{th} .

factors, the scattering intensity is given by [9]

$$I(\Omega) = (1/Z) \sum_{I,F} e^{-\beta E_I} |M_{F,I}|^2 \delta(E_I - E_F + \Omega),$$

where Z is the partition function, β is inverse temperature, $\Omega = \omega_i - \omega_f$ is the Raman shift, $\omega_{i,f}$ are the in and out photon frequencies with polarizations $\hat{e}_{i,f}$, and $E_{I,F}$ are the energies of the initial and final states. We assume that the low-energy effective theory describing the system has bandwidth $D \ll \bar{\omega}$, where $\bar{\omega} = (\omega_i + \omega_f)/2$. In most cases of interest $D/\bar{\omega} \sim 0.1$ or less. Then, the matrix element $M_{F,I}$ can be approximated by [for details see the Supplementary Material (SM)]

$$M_{F,I} \approx \sum_{\alpha,\beta} (e_{i,\alpha} e_{f,\beta}^*) \langle F | (\hat{v}_{\alpha\beta} - [\hat{v}_\alpha, \hat{v}_\beta]/\bar{\omega}) | I \rangle. \quad (1)$$

Here $\hat{v}_\alpha \equiv \partial\mathcal{H}/\partial k_\alpha$ and $\hat{v}_{\alpha\beta} \equiv \partial^2\mathcal{H}/(\partial k_\alpha \partial k_\beta)$ are the paramagnetic and diamagnetic currents, respectively, \mathcal{H} is the Hamiltonian and \mathbf{k} the wavevector.

We consider a quasi two-dimensional system for which $I_{x_\theta y_\theta}(\Omega)$ is the Raman intensity for in and out polarizations along \hat{x}_θ and \hat{y}_θ , respectively, with $\hat{x} \cdot \hat{x}_\theta = \cos\theta$, as shown in Fig. 1(a). The angle dependent antisymmetric Raman intensity can be expressed as (see SM for details)

$$I_A(\Omega, \theta) = 2 \cos(2\theta) I_{A_{2g}}^{B_{2g}}(\Omega) - 2 \sin(2\theta) I_{A_{2g}}^{B_{1g}}(\Omega), \quad (2)$$

where

$$I_{A_{2g}}^i(\Omega) \equiv (1/Z) \sum_{I,F} e^{-\beta E_I} \delta(E_I - E_F + \Omega) \times \left[\langle I | \hat{\Gamma}_{A_{2g}} | F \rangle \langle F | \hat{\Gamma}_i | I \rangle - \langle I | \hat{\Gamma}_i | F \rangle \langle F | \hat{\Gamma}_{A_{2g}} | I \rangle \right], \quad (3)$$

with $i = (B_{1g}, B_{2g})$. The Raman operators $\hat{\Gamma}_{A_{2g}} \equiv [\hat{v}_x, \hat{v}_y]/\bar{\omega}$ [24, 25], $\hat{\Gamma}_{B_{1g}} \equiv (\hat{v}_{xx} - \hat{v}_{yy})/2$ and $\hat{\Gamma}_{B_{2g}} \equiv \hat{v}_{xy}$. Note, $\hat{\Gamma}_{A_{2g}}$ is an antisymmetric rank two tensor and is an antihermitian operator, while $\hat{\Gamma}_i$ are symmetric rank two tensors and Hermitian operators.

Two comments are in order. First, the commutator $\hat{\Gamma}_{A_{2g}}$ is non-zero only for multi-orbital systems, and it cannot be constructed within the widely-used effective mass approximation that neglects the paramagnetic current [9]. Moreover, antihermiticity enforces that $\hat{\Gamma}_{A_{2g}}$ has only interband terms of the type $(c_{\mathbf{k},1}^\dagger c_{\mathbf{k},2} - c_{\mathbf{k},2}^\dagger c_{\mathbf{k},1})$ between bands 1, 2. This ensures that antisymmetric responses have no intraband contribution. Second, since $A_{2g} \otimes B_{2g} = B_{1g}$, finite $I_{A_{2g}}^{B_{2g}}(\Omega)$ implies broken reflection symmetries $M_{x'} : (x, y) \rightarrow (y, x)$ and $M_{y'} : (x, y) \rightarrow (-y, -x)$, where (x', y') are $\pi/4$ rotated counterclockwise with respect to (x, y) . Likewise, finite $I_{A_{2g}}^{B_{1g}}(\Omega)$ implies broken reflections $M_x : (x, y) \rightarrow (x, -y)$ and $M_y : (x, y) \rightarrow (-x, y)$. Thus, even though we use tetragonal notation, antisymmetric Raman response is finite only for orthorhombic or lower symmetry systems.

Fluctuation dissipation relation.— The next step is to identify the susceptibilities that can be extracted from $I_A(\Omega, \theta)$. For this we define the imaginary time ordered function $\chi_{A_{2g}}^i(\tau) \equiv -\langle T_\tau \hat{\Gamma}_{A_{2g}}(\tau) \hat{\Gamma}_i(0) \rangle$, over the interval $\tau = [-\beta, \beta]$, and its Fourier transform by $\chi_{A_{2g}}^i(\Omega) = (1/\beta) \sum_{\Omega_n} \chi_{A_{2g}}^i(i\Omega_n) e^{-i\Omega_n \tau}$ in terms of bosonic Matsubara frequencies Ω_n . Here $\langle \dots \rangle$ implies thermodynamic average. We also define the related cross-susceptibility $\phi_{A_{2g}}^i(i\Omega_n) \equiv \chi_{A_{2g}}^i(i\Omega_n) - \chi_{A_{2g}}^i(-i\Omega_n)$. Note, by definition, $\chi_{A_{2g}}^i(-i\Omega_n) = \chi_{A_{2g}}^{A_{2g}}(i\Omega_n)$. Using Lehmann representation we get (see SM for details)

$$\phi_{A_{2g}}^i(i\Omega_n) = \frac{1}{Z} \sum_{n,m} \left[(\hat{\Gamma}_{A_{2g}})_{nm} (\hat{\Gamma}_i)_{mn} - (\hat{\Gamma}_i)_{nm} (\hat{\Gamma}_{A_{2g}})_{mn} \right] \times (e^{-\beta E_n} - e^{\beta E_m}) / (i\Omega_n + E_n - E_m), \quad (4)$$

where $(\hat{O})_{nm} \equiv \langle n | \hat{O} | m \rangle$. Comparing Eqs. (3) and (4) we obtain the fluctuation-dissipation relation

$$I_{A_{2g}}^i(\Omega) = -(1/\pi) [1 + n_B(\Omega)] \text{Im} \phi_{A_{2g}}^i(\Omega + i\eta), \quad (5)$$

where $n_B(\Omega) \equiv 1/(e^{\beta\Omega} - 1)$ is the Bose function. By contrast, once symmetry resolved, standard Raman response gives the auto-susceptibility $\text{Im} \chi_j^j(\Omega + i\eta)$, where $\chi_j^j(\tau) \equiv -\langle T_\tau \hat{\Gamma}_j(\tau) \hat{\Gamma}_j(0) \rangle$, and $j = (A_{1g}, B_{1g}, B_{2g}, A_{2g})$. Consequently, it cannot detect reflection symmetry breaking.

General properties.— We now compare the properties of $\phi_{A_{2g}}^i(i\Omega_n)$ extracted from antisymmetric Raman response with those of $\chi_j^j(i\Omega_n)$.

(i) Eq. (4) implies $\phi_{A_{2g}}^i(\Omega + i\eta)^* = \phi_{A_{2g}}^i(\Omega - i\eta)$, using the antihermiticity of $\hat{\Gamma}_{A_{2g}}$. Moreover, $\phi_{A_{2g}}^i(i\Omega_n)$ is odd in Ω_n . Thus, the real and the imaginary parts of $\phi_{A_{2g}}^i(\Omega + i\eta)$ are odd and even functions of Ω , respectively. It is opposite in case of $\chi_j^j(\Omega + i\eta)$, as shown in Fig. 1(c, d).

(ii) From the detailed balance relation [26] $I_{y_\theta x_\theta}(-\Omega) = e^{-\beta\Omega} I_{x_\theta y_\theta}(\Omega)$ (see SM for details), we get $I_A(\Omega \rightarrow 0, \theta) \rightarrow 0$. Since $n_B(\Omega) \propto 1/\Omega$ in this limit, we have $\lim_{\Omega \rightarrow 0} \text{Im} \phi_{A_{2g}}^i(\Omega + i\eta) \sim |\Omega|^\gamma$ with $\gamma > 1$. As discussed later, in practice $\text{Im} \phi_{A_{2g}}^i(\Omega + i\eta)$ from electronic excitations [one loop graph in Fig. 1(b)] is zero below a threshold, as shown in Fig. 1(c). Under suitable conditions a collective mode [two loop graph in Fig. 1(b)] can appear inside this spectroscopic ‘‘gap’’.

(iii) From Eq. (4) we obtain

$$\int_{-\infty}^{\infty} \frac{d\Omega}{2\pi} \phi_{A_{2g}}^i(\Omega + i\eta) = \langle [\hat{\Gamma}_i, \hat{\Gamma}_{A_{2g}}] \rangle. \quad (6)$$

Since the right hand side is zero for a tetragonal system, it acts as an order parameter for reflection symmetry breaking which can be extracted from spectroscopy. By contrast, in standard Raman the frequency integral of $\text{Im} \chi_j^j(\Omega + i\eta)/\Omega$ is related to a static susceptibility by Kramers-Kronig relation [11, 27].

(iv) Reciprocity relation: We define the correlation function $C_{A_{2g}}^i(t) \equiv \langle \hat{\Gamma}_{A_{2g}}(t) \hat{\Gamma}_i(0) \rangle$ and $C_{A_{2g}}^i(\Omega) \equiv \int_{-\infty}^{\infty} dt \exp(i\Omega t) C_{A_{2g}}^i(t)$, and likewise $C_i^{A_{2g}}(t)$ and $C_i^{A_{2g}}(\Omega)$. The antisymmetric Raman intensities are given by $I_{A_{2g}}^i(\Omega) = C_{A_{2g}}^i(\Omega) - C_i^{A_{2g}}(\Omega)$. We consider a time reversal symmetric system in an external magnetic field \mathbf{h} . As the Raman operators are even under time reversal, and $\hat{\Gamma}_{A_{2g}}$ is antihermitian, one can show that $C_{A_{2g}}^i(t, \mathbf{h}) = -C_i^{A_{2g}}(t, -\mathbf{h})$. This gives the *reciprocity relation* (see SM for details)

$$I_{A_{2g}}^i(\Omega, \mathbf{h}) = I_{A_{2g}}^i(\Omega, -\mathbf{h}). \quad (7)$$

A violation of the above was reported recently for the CDW phase of GdTe₃ [14].

Raman cross-susceptibilities $B_{1g} \otimes B_{2g}$ or $E_g^1 \otimes E_g^2$ are obtained by subtracting right-left circular polarizations signal from the left-right one in reference tetragonal or hexagonal systems, respectively [28, 29]. However, they do not involve the A_{2g} -operator, and hence they do not have the features discussed in this work.

Examples.— Having discussed the general properties of $\phi_{A_{2g}}^i$, we illustrate them with examples from systems of current interest.

(1) *Electronic continuum.*— This example is taken to illustrate the antisymmetric Raman response of a normal metal. We consider a tight binding Hamiltonian of (p_x, p_y) orbitals that is often studied in the context of the tritellurides [30–32]. It is given by $\mathcal{H}_0 = \sum_{\mathbf{k}} h_{\mathbf{k}}$,

$$h_{\mathbf{k}} = \sum_{\nu=x,y} \epsilon_{\mathbf{k},\nu} c_{\mathbf{k},\nu}^\dagger c_{\mathbf{k},\nu} + V_{\mathbf{k}} c_{\mathbf{k},x}^\dagger c_{\mathbf{k},y} + \text{h.c.},$$

with $\epsilon_{\mathbf{k},x} = -2t_1 \cos k_x + 2t_2 \cos k_y - \mu$, $\epsilon_{\mathbf{k},y} = \epsilon_{\mathbf{k},x}(k_x \leftrightarrow k_y)$, and $V_{\mathbf{k}} = -2V_0 \sin k_x \sin k_y - \epsilon_m \cos k_x \cos k_y$. The ϵ_m -term breaks (M_x, M_y) symmetries, while $(M_{x'}, M_{y'})$ are intact, making the system orthorhombic with finite $\phi_{A_{2g}}^{B_{1g}}(\Omega)$ and zero $\phi_{A_{2g}}^{B_{2g}}(\Omega)$. In Fig. 1(c) we show $\phi_{A_{2g}}^{B_{1g}}(\Omega)$ for a standard set of parameters and compare it with $\chi_{B_{1g}}^{B_{1g}}(\Omega)$ in Fig. 1(d). The former has three striking features. First, the magnitude of $\phi_{A_{2g}}^{B_{1g}}$ is an order of magnitude smaller than $\chi_{B_{1g}}^{B_{1g}}$, a result of the small parameter $D/\bar{\omega}$. Second, the absence of intraband Drude contribution in $\text{Im}\phi_{A_{2g}}^{B_{1g}}(\Omega)$, which is imposed by $\hat{\Gamma}_{A_{2g}}$. Third, the same is non-zero only above a threshold frequency Ω_{th} . This is typical of orthorhombic (and lower symmetry) systems where all band degeneracies are lifted (the irreducible representations of the point group are one dimensional). This implies that interband particle-hole excitations need a minimum energy $\Omega_{th} \sim 2V_0$ in this model. Thus the antisymmetric response has a spectroscopic “gap” even though the system is metallic and, in principle, one can observe a collective mode of a broken symmetry phase in this gap.

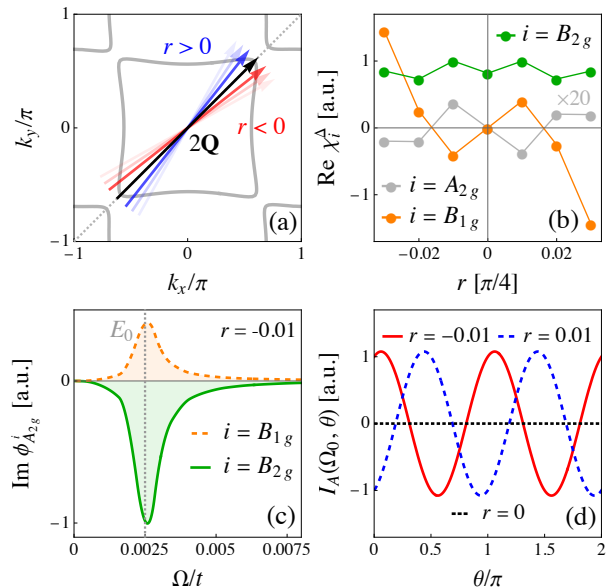


FIG. 2. (Color Online) (a) Fermi surface of the tritellurides for $T > T_c$. $2\mathbf{Q}$ is the CDW wavevector. It is tilted by an angle r compared to the direction $x = y$. (b) Dependence of various susceptibilities as a function of r . By symmetry, $\text{Re}\chi_{A_{2g}}^{\Delta}(E_0) = \text{Re}\chi_{B_{1g}}^{\Delta}(E_0) = 0$ for $r = 0$. A finite r is necessary to explain the monoclinicity of the $T < T_c$ phase. (c) Antisymmetric Raman responses due to the amplitude mode of the CDW. The absolute signs of the two responses and their relative strengths are consistent with the experiments. (d) Angular variation of the antisymmetric Raman intensity, and its dependence on the sign of r .

(2) *Amplitude mode of CDW.*— We explain how the collective mode of a CDW, with energy E_0 , appears in an antisymmetric channel, as recently reported for the tritellurides [12]. We also discuss the microscopic information that can be extracted from such observation.

All the available Raman studies [12, 14, 33] on the tritellurides show similar collective mode features. Using notations developed here they can be summarized as follows. (i) $I_A(E_0, 0) > 0$, which implies $\text{Im}\phi_{A_{2g}}^{B_{2g}}(E_0) < 0$; (ii) $I_A(E_0, \pi/4) < 0$, implying $\text{Im}\phi_{A_{2g}}^{B_{1g}}(E_0) > 0$; and (iii) $I_A(E_0, 0) \gg |I_A(E_0, \pi/4)|$, which gives $|\text{Im}\phi_{A_{2g}}^{B_{2g}}(E_0)| \gg \text{Im}\phi_{A_{2g}}^{B_{1g}}(E_0) > 0$. Our goal is to model these features and draw conclusions about the CDW state.

The coupling of light to a charge neutral CDW amplitude mode involve two fermion loops [3, 34–36], as shown in Fig. 1(b). Since each loop is nonzero, all four mirror symmetries of a reference tetragonal system have to be broken. Thus, observing the collective mode implies monoclinicity. The tritellurides are orthorhombic to begin with broken mirrors (M_x, M_y) in the normal state at temperature $T > T_c$, the CDW transition temperature. Thus, the CDW breaks the mirrors $(M_{x'}, M_{y'})$

along with lattice translation symmetry [32]. We postulate that the former is due to a tilt of the ordering wavevector $2\mathbf{Q}$ from the high-symmetry direction $x = y$, at an angle $(1+r)\pi/4$ from the x -axis, with r the tilt parameter as shown in Fig. 2(a) along with the normal state Fermi surface. Note, the precise origin of the monoclinicity is not important for what follows, and other possibilities have been discussed [13, 32].

Experimentally, E_0 is about two orders of magnitude smaller than the tight-binding scales [16–19], and it lies well inside the interband “gap” discussed in example (1). Thus, $\text{Im}\chi_{A_{2g}}^{\Delta}(E_0) = 0$, and

$$\text{Im}\phi_{A_{2g}}^i(\Omega \sim E_0) \approx 2[\text{Re}\chi_{A_{2g}}^{\Delta}(\Omega)][\text{Re}\chi_{\Delta}^i(\Omega)]\text{Im}D(\Omega), \quad (8)$$

where $D(\Omega) = 2E_0/[(\Omega + i\gamma_0)^2 - E_0^2]$ is the amplitude mode propagator, with γ_0 its broadening. This relation applied to the experimental implication (iii) discussed above gives $|\text{Re}\chi_{\Delta}^{B_{2g}}(E_0)| \gg |\text{Re}\chi_{\Delta}^{B_{1g}}(E_0)|$. In turn, it indicates that the CDW order parameter is predominantly of the inter-orbital type with a B_{2g} character.

The above suggests that the CDW phase can be described by the mean field Hamiltonian $\mathcal{H} = \mathcal{H}_0 + \Delta \sum_{\mathbf{k}} [c_{\mathbf{k}+\mathbf{Q},x}^{\dagger} c_{\mathbf{k}-\mathbf{Q},y} + c_{\mathbf{k}+\mathbf{Q},y}^{\dagger} c_{\mathbf{k}-\mathbf{Q},x} + \text{h.c.}]$, where \mathcal{H}_0 is that of example (1), and Δ is the CDW potential with $2\mathbf{Q}$ ordering wavevector. The amplitude mode describes fluctuations of Δ hybridized with the phonon that triggers the CDW instability [35–38]. The hybridization implies that $E_0 \neq \Delta$. The computational details are given in the SM. Note, $\text{Re}\chi_{\Delta}^i(E_0) = \text{Re}\chi_{\Delta}^i(E_0)$ for $i = (B_{1g}, B_{2g})$, while $\text{Re}\chi_{A_{2g}}^{\Delta}(E_0) = -\text{Re}\chi_{B_{1g}}^{\Delta}(E_0)$. In Fig. 2(b) we show the tilt angle r dependence of $\text{Re}\chi_{\Delta}^i(E_0)$ for $i = (A_{2g}, B_{1g}, B_{2g})$. Since Δ is a B_{2g} variable for $r = 0$, we get $\text{Re}\chi_{A_{2g}}^{\Delta}(E_0) = \text{Re}\chi_{B_{1g}}^{\Delta}(E_0) = 0$ in this limit. By contrast, $\text{Re}\chi_{B_{2g}}^{\Delta}(E_0)$ is nearly independent of r .

In Fig. 2(c) we show the amplitude mode in the two antisymmetric Raman channels with their absolute signs and relative magnitudes consistent with the experiments. Since $\phi_{A_{2g}}^{B_{2g}}$ is a B_{1g} quantity, it is proportional to r , and the fact $\text{Im}\phi_{A_{2g}}^{B_{2g}}(E_0) < 0$ (the monoclinic domains are pinned to the orthorhombic ones) is consistent with $r < 0$ in the model. We find that the remaining two properties, namely $\text{Im}\phi_{A_{2g}}^{B_{1g}}(E_0) > 0$ and $|\text{Im}\phi_{A_{2g}}^{B_{2g}}(E_0)| \gg |\text{Im}\phi_{A_{2g}}^{B_{1g}}(E_0)|$ depend on microscopic details, and they could be obtained only by fine tuning \mathcal{H} . Finally, Fig. 2(d) shows the two-fold symmetric angular dependence of the antisymmetric Raman intensity as defined by Eq. (2). The two cases $r < 0$ and $r > 0$ are $\pi/2$ phase shifted because, with sign change of r , the sign of $\text{Im}\phi_{A_{2g}}^{B_{2g}}(E_0)$ changes but not that of $\text{Im}\phi_{A_{2g}}^{B_{1g}}(E_0)$.

Thus, signals of collective modes in antisymmetric Raman channels yield several useful microscopic properties that cannot be accessed otherwise.

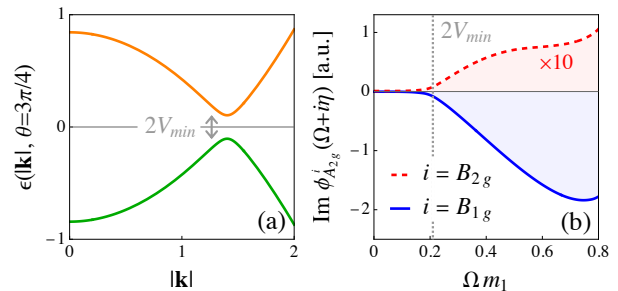


FIG. 3. (Color Online) (a) Band dispersions of an excitonic insulator in polar coordinates, with minimum charge gap of $2V_{\min}$. (b) Antisymmetric Raman spectra in this phase with $\Omega_{th} = 2V_{\min}$. Integrated weight of $\text{Im}\phi_{A_{2g}}^{B_{1g}}(\Omega)$ measures electronic monoclinicity.

(3) *Exciton insulator.*— Ta_2NiSe_5 , which has attracted considerable interest in recent times, undergoes a transition from a high- T orthorhombic metal to a low- T monoclinic insulator due to the formation of excitons, or particle-hole pairs [20–23]. Our goal is to illustrate that antisymmetric Raman response will be an interesting probe of this and other similar insulating systems.

We model the metallic phase by two bands $\pm\epsilon_{\mathbf{k}}$ with $\epsilon_{\mathbf{k}} = k_x^2/(2m_1) + k_y^2/(2m_2) - E_0$, with $m_1 \neq m_2$ that breaks mirrors ($M_{x'}, M_{y'}$). In this phase $\phi_{A_{2g}}^{B_{1g}}$ vanishes, while $\phi_{A_{2g}}^{B_{2g}}$ is nonzero (zero in this simplified model). In the insulating phase the bands have finite hybridization $V_{\mathbf{k}} = (k_x k_y + c)/m$, which opens a gap and breaks the mirrors (M_x, M_y) as well, making $\phi_{A_{2g}}^{B_{1g}}$ non-zero. We show its imaginary part in Fig. 2, where $\Omega_{th} \sim 2V_{\min}$ is now a measure of the charge gap. Furthermore, since lattice strain effects are absent in Raman response [11, 39], the electronic monoclinicity can be extracted from the integrated spectrum using Eq. (6).

Conclusion.— Antisymmetric Raman response measures cross-susceptibilities of two Raman operators, of which one is $\hat{\Gamma}_{A_{2g}}$ that filters out intraband excitations. The spectra have “gaps” below a threshold which measures minimum interband excitation energy in metals and the charge gap in insulators. It can detect subtle mirror symmetry breaking such as CDW transitions in tritellurides and excitonic insulator transition in Ta_2NiSe_5 . In symmetry broken phases a collective mode can appear inside the gap which has microscopic information such as the orbital character of the order parameter. Thus, antisymmetric Raman response is a powerful tool to probe low symmetry materials, both metallic and insulating.

Acknowledgement.— We are thankful to T. Freitas, Y. Gallais, and A. Meszaros for insightful discussions. We acknowledge financial support from French Agence Nationale de la Recherche (ANR) grant ANR-23-CE30-0030 (SUPER2DTMD).

-
- [1] A. A. Abrikosov and L. A. Falkovskii, *Sov. Phys. JETP* **13**, 179 (1961).
- [2] A. A. Abrikosov and V. M. Genkin, *Sov. Phys. JETP* **38**, 417 (1961).
- [3] M. V. Klein, *Phys. Rev. B* **25**, 7192 (1982).
- [4] M. Balkanski, R. F. Wallis, and E. Haro, *Phys. Rev. B* **28**, 1928 (1983).
- [5] M. V. Klein and S. B. Dierker, *Phys. Rev. B* **29**, 4976 (1984).
- [6] B. S. Shastry and B. I. Shraiman, *Phys. Rev. Lett.* **65**, 1068 (1990).
- [7] B. S. Shastry and B. I. Shraiman, *Int. J. Mod. Phys.* **5**, 365 (1991).
- [8] W. Hayes and R. Loudon, *Scattering of Light by Crystals*, Dover Publications, 2004.
- [9] for a review see, e.g., T. P. Devereaux and R. Hackl, *Rev. Mod. Phys.* **79**, 175 (2007).
- [10] A. Sacuto, Y. Gallais, M. Cazayous, M.-A. Méasson, G. D. Gu, and D. Colson, *Rep. Prog. Phys.* **76**, 022502 (2013).
- [11] Y. Gallais and I. Paul, *Comptes Rendus Physique* **17**, 113 (2016).
- [12] Y. Wang, I. Petrides, G. McNamara, M. M. Hosen, S. Lei, Y.-C. Wu, J. L. Hart, H. Lv, J. Yan, D. Xiao, J. J. Cha, P. Narang, L. M. Schoop, and K. S. Burch, *Nat.* **606**, 896 (2022).
- [13] B. Singh, G. McNamara, K.-M. Kim, S. Siddique, S. D. Funni, W. Zhang, X. Luo, P. Sakrikar, E. M. Kenney, R. Singha, S. Alekseev, S. A. A. Ghorashi, T. J. Hicken, C. Baines, H. Luetkens, Y. Wang, V. M. Plisson, M. Geiwitz, C. A. Occhialini, R. Comin, M. J. Graf, L. Zhao, J. Cano, R. M. Fernandes, J. J. Cha, L. M. Schoop, and K. S. Burch, arXiv:2411.08322.
- [14] D. Wulferding, J. Park, T. Tohyama, S. R. Park, and C. Kim, *Nat. Commun.* **16**, 114 (2025).
- [15] M. Lavagnini, H. -M. Eiter, L. Tassini, B. Muschler, R. Hackl, R. Monnier, J. -H. Chu, I. R. Fisher, and L. Degiorgi, *Phys. Rev. B* **81**, 081101(R) (2010).
- [16] V. Brouet, W. L. Yang, X. J. Zhou, Z. Hussain, N. Ru, K. Y. Shin, I. R. Fisher, Z. X. Shen, *Phys. Rev. Lett.* **93**, 126405 (2004).
- [17] V. Brouet, W. L. Yang, X. J. Zhou, Z. Hussain, R. G. Moore, R. He, D. H. Lu, Z. X. Shen, J. Laverock, S. Dugdale, N. Ru, and I. R. Fisher, *Phys. Rev. B* **77**, 235104 (2008).
- [18] R. G. Moore, V. Brouet, R. He, D. H. Lu, N. Ru, J. -H. Chu, I. R. Fisher, Z. -X. Shen, *Phys. Rev. B* **81**, 073102 (2010).
- [19] A. Gallo-Frantz, A. A. Sinchenko, D. Ghoneim, L. Ortega, P. Godard, P.-O. Renault, P. Grigoriev, A. Hadj-Azzem, P. Monceau, D. Thiaudière, E. Bellec, V. L. R. Jacques, D. Le Bolloc'h, *Nat. Comm* **15**, 3665 92024).
- [20] F. D. Salvo, C. Chen, R. Fleming, J. Waszczak, R. Dunn, S. Sunshine, and J. A. Ibers, *J. Less Common Metals* **116**, 51 (1986).
- [21] Y. F. Lu, H. Kono, T. I. Larkin, A. W. Rost, T. Takayama, A. V. Boris, B. Keimer, and H. Takagi, *Nat. Comm.* **8**, 14408 (2017).
- [22] G. Mazza, M. Rösner, L. Windgätter, S. Latini, H. Hübener, A. J. Millis, A. Rubio, and A. Georges, *Phys. Rev. Lett.* **124**, 197601 (2020).
- [23] for a review see, e.g., T. Kaneko and Y. Ohta, *J. Phys. Soc. Jpn.* **94**, 012001 (2025).
- [24] C. S. Farias, M.-A. Méasson, A. Ferraz, and S. Burdin, *Phys. Rev. B* **101**, 205114 (2020).
- [25] E. Riccardi, O. Kashuba, M. Cazayous, M.-A. Méasson, A. Sacuto, and Y. Gallais, *Phys. Rev. Materials* **3**, 014002 (2019).
- [26] R. Loudon, *J. Raman Spectroscop.* **7**, 10 (1978).
- [27] Y. Gallais, R. M. Fernandes, I. Paul, L. Chauviere, Y. -X. Yang, M. -A. Measson, M. Cazayous, A. Sacuto, D. Colson, and A. Forget, *Phys. Rev. Lett.* **111**, 267001 (2013).
- [28] H. F. Yang, K. Y. He, J. Koo, S. W. Shen, S. H. Zhang, G. Liu, Y. Z. Liu, C. Chen, A. J. Liang, K. Huang, M. X. Wang, J. J. Gao, X. Luo, L. X. Yang, J. P. Liu, Y. P. Sun, S. C. Yan, B. H. Yan, Y. L. Chen, X. Xi, and Z. K. Liu, *Phys. Rev. Lett.* **129**, 156401 (2022).
- [29] W. Qi, J. Dong, S. Ponzoni, G. Huitric, R. Grasset, Y. Laplace, L. Cario, M. Marsi, E. Papalazarou, A. Zobelli, A. Alekhin, Y. Gallais, A. Bendounan, and L. Perfetti, *Nano Lett.* **24**, 13134 92024).
- [30] H. Yao, J. A. Robertson, E.-A. Kim, and S. A. Kivelson, *Phys. Rev. B* **74**, 245126 (2006).
- [31] H. -M. Eiter, M. Lavagnini, R. Hackl, E. A. Nowadnick, A. F. Kemper, T. P. Devereaux, J. -H. Chu, J. G. Analytis, I. R. Fisher, and L. Degiorgi, *PNAS* **110**, 64 (2013).
- [32] S. Alekseev, S. A. A. Ghorashi, R. M. Fernandes, and J. Cano, *Phys. Rev. B* **110**, 205103 (2024).
- [33] T. Freitas and Y. Gallais, private communication.
- [34] P. A. Lee, T. M. Rice, and P. W. Anderson, *Solid State Comm.* **14**, 703 (1974).
- [35] T. Cea and L. Benfatto, *Phys. Rev. B* **90**, 224515 (2014).
- [36] M. Udina, T. Cea, and L. Benfatto, *Phys. Rev. B* **100**, 165131 (2019).
- [37] M. Maschek, S. Rosenkranz, R. Heid, A. H. Said, P. Giraldo-Gallo, I. R. Fisher, and F. Weber, *Phys. Rev. B* **91**, 235146 (2015).
- [38] R. Grasset, T. Cea, Y. Gallais, M. Cazayous, A. Sacuto, L. Cario, L. Benfatto, and M.-A. Méasson, *Phys. Rev. B* **97**, 094502 (2018).
- [39] Y. Gallais, I. Paul, L. Chauviere, and J. Schmalian, *Phys. Rev. Lett.* **116**, 017001 (2016).

SUPPLEMENTARY INFORMATION

Derivation of Eq. (1)

In general, the Raman matrix element is given by

$$M_{F,I} = \sum_{\alpha,\beta} (e_{i,\alpha} e_{f,\beta}^*) \left[\langle F | \hat{v}_{\alpha\beta} | I \rangle + \sum_M \frac{\langle F | \hat{v}_\alpha | M \rangle \langle M | \hat{v}_\beta | I \rangle}{E_I - E_M - \omega_f} + \frac{\langle F | \hat{v}_\beta | M \rangle \langle M | \hat{v}_\alpha | I \rangle}{E_I - E_M + \omega_i} \right], \quad (\text{S1})$$

where $\Omega = \omega_i - \omega_f$ is the Raman shift, $\omega_{i,f}$ are the in and out photon frequencies with polarizations $\hat{e}_{i,f}$. We assume that the bandwidth of the effective theory $D \ll \omega_i, \omega_f$. Since $(E_I - E_M) < D$, we can neglect it in the denominators, and the intermediate states M can be summed to unity. Writing $\omega_{i,f} = \bar{\omega} \pm \Omega/2$, and neglecting $\Omega/\bar{\omega}$ we get Eq. (1) of the main text.

Derivation of Eqs. (2) and (3)

We consider the scattering geometry where the in-coming photon polarization is $\hat{e}_i = \hat{x}_\theta = \cos(\theta)\hat{x} + \sin(\theta)\hat{y}$, and the out-going photon polarization is $\hat{e}_f = \hat{y}_\theta = -\sin(\theta)\hat{x} + \cos(\theta)\hat{y}$. The associated Raman matrix element can be written

$$M_{F,I}(\theta) = \langle F | \hat{D}(\theta) + \hat{P}(\theta) | I \rangle, \quad (\text{S2})$$

where the diamagnetic term is

$$\hat{D}(\theta) = \cos(2\theta)\hat{\Gamma}_{B_{2g}} - \sin(2\theta)\hat{\Gamma}_{B_{1g}},$$

and the paramagnetic term is

$$\hat{P}(\theta) = -\hat{\Gamma}_{A_{2g}},$$

with $\hat{\Gamma}_{A_{2g}} \equiv [\hat{v}_x, \hat{v}_y]/\bar{\omega}$, $\hat{\Gamma}_{B_{1g}} \equiv (\hat{v}_{xx} - \hat{v}_{yy})/2$ and $\hat{\Gamma}_{B_{2g}} \equiv \hat{v}_{xy}$. We need to compare this scattering geometry with the one obtained by interchanging the in and out polarization directions. Denoting the Raman matrix element of the latter by $M_{F,I}(\theta_\perp)$, we get

$$M_{F,I}(\theta_\perp) = \langle F | \hat{D}(\theta) - \hat{P}(\theta) | I \rangle. \quad (\text{S3})$$

Thus, the antisymmetric Raman response is

$$\begin{aligned} I_A(\Omega, \theta) &= I_{x_\theta y_\theta}(\Omega) - I_{y_\theta y_\theta}(\Omega) \\ &= \frac{1}{Z} \sum_{I,F} e^{-\beta E_I} \delta(E_I - E_F + \Omega) \\ &\quad \times [|M_{F,I}(\theta)|^2 - |M_{F,I}(\theta_\perp)|^2]. \end{aligned} \quad (\text{S4})$$

Noting that $\hat{P}(\theta)$ is antihermitian, from the above we get Eqs. (2) and (3) of the main text.

Derivation of Eq. (4)

The imaginary time ordered function $\chi_{A_{2g}}^i(\tau) \equiv -\langle T_\tau \hat{\Gamma}_{A_{2g}}(\tau) \hat{\Gamma}_i(0) \rangle$, can be expressed in the Lehmann basis as

$$\chi_{A_{2g}}^i(\tau) = -\theta(\tau) \frac{1}{Z} \sum_{n,m} e^{-\beta E_n} (\hat{\Gamma}_{A_{2g}})_{nm} (\hat{\Gamma}_i)_{mn} e^{\tau(E_n - E_m)}$$

$$-\theta(-\tau) \frac{1}{Z} \sum_{n,m} e^{-\beta E_n} (\hat{\Gamma}_i)_{nm} (\hat{\Gamma}_{A_{2g}})_{mn} e^{\tau(E_m - E_n)}, \quad (\text{S5})$$

where τ is defined over the interval $[-\beta, \beta]$. From the above we deduce that $\chi_{A_{2g}}^i(\tau > 0) = \chi_{A_{2g}}^i(\tau - \beta < 0)$ and, in particular, $\chi_{A_{2g}}^i(\beta) = \chi_{A_{2g}}^i(0)$. The periodic boundary condition implies that $\chi_{A_{2g}}^i(\tau)$ can be expanded in bosonic Matsubara frequency. We get

$$\begin{aligned} \chi_{A_{2g}}^i(i\Omega_n) &= \int_0^\beta d\tau e^{i\Omega_n \tau} \chi_{A_{2g}}^i(\tau) \\ &= \frac{1}{Z} \sum_{n,m} (\hat{\Gamma}_{A_{2g}})_{nm} (\hat{\Gamma}_i)_{mn} \frac{e^{-\beta E_n} - e^{-\beta E_m}}{i\Omega_n + E_n - E_m}. \end{aligned} \quad (\text{S6})$$

This implies that

$$\begin{aligned} \phi_{A_{2g}}^i(i\Omega_n) &= \chi_{A_{2g}}^i(i\Omega_n) - \chi_{A_{2g}}^i(-i\Omega_n) \\ &= \frac{1}{Z} \sum_{n,m} [(\hat{\Gamma}_{A_{2g}})_{nm} (\hat{\Gamma}_i)_{mn} - (\hat{\Gamma}_i)_{nm} (\hat{\Gamma}_{A_{2g}})_{mn}] \\ &\quad \times \frac{e^{-\beta E_n} - e^{\beta E_m}}{i\Omega_n + E_n - E_m}, \end{aligned} \quad (\text{S7})$$

which is Eq. (4) of the main text.

Comparing Stokes and anti-Stokes processes

We consider a Raman scattering process where the in-photon has frequency and polarization ω_1 and $\hat{\alpha}$, respectively, while for the out-photon they are ω_2 and $\hat{\beta}$, respectively. We take $\Omega = \omega_1 - \omega_2 > 0$, i.e., this is a Stokes process. The scattering intensity for this process is given by

$$I_{\alpha\beta}(\omega_1, \omega_2) = \frac{1}{Z} \sum_{i,f,m} e^{-\beta E_i} \delta(E_i - E_f + \Omega) \left| M_{fi}^{\alpha\beta}(\omega_1, \omega_2) \right|^2,$$

where

$$M_{fi}^{\alpha\beta}(\omega_1, \omega_2) = (\hat{v}_{\alpha\beta})_{fi} + \frac{(\hat{v}_\alpha)_{fm} (\hat{v}_\beta)_{mi}}{E_{im} - \omega_2} + \frac{(\hat{v}_\beta)_{fm} (\hat{v}_\alpha)_{mi}}{E_{im} + \omega_1}, \quad (\text{S8})$$

with $E_{im} \equiv E_i - E_m$. This intensity is to be compared with an anti-Stokes process where the in-photon has frequency and polarization ω_2 and $\hat{\beta}$, respectively, while those for the out-photon are ω_1 and $\hat{\alpha}$, respectively. The intensity of this process is

$$I_{\beta\alpha}(\omega_2, \omega_1) = \frac{1}{Z} \sum_{i,f,m} e^{-\beta E_i} \delta(E_i - E_f - \Omega) \left| M_{fi}^{\beta\alpha}(\omega_2, \omega_1) \right|^2,$$

where

$$M_{fi}^{\beta\alpha}(\omega_2, \omega_1) = (\hat{v}_{\beta\alpha})_{fi} + \frac{(\hat{v}_\beta)_{fm} (\hat{v}_\alpha)_{mi}}{E_{im} - \omega_1} + \frac{(\hat{v}_\alpha)_{fm} (\hat{v}_\beta)_{mi}}{E_{im} + \omega_2} \quad (\text{S9})$$

Using energy conservation relation $E_i + \omega_2 = E_f + \omega_1$ the anti-Stokes matrix element can be re-written as

$$M_{fi}^{\beta\alpha}(\omega_2, \omega_1) = (\hat{v}_{\beta\alpha})_{fi} + \frac{(\hat{v}_\beta)_{fm} (\hat{v}_\alpha)_{mi}}{E_{fm} - \omega_2} + \frac{(\hat{v}_\alpha)_{fm} (\hat{v}_\beta)_{mi}}{E_{fm} + \omega_1}$$

$$\begin{aligned}
&= \left[(\hat{v}_{\alpha\beta})_{if} + \frac{(\hat{v}_\alpha)_{im}(\hat{v}_\beta)_{mf}}{E_{fm} - \omega_2} + \frac{(\hat{v}_\beta)_{im}(\hat{v}_\alpha)_{mf}}{E_{fm} + \omega_1} \right]^* \\
&= \left[M_{if}^{\alpha\beta}(\omega_1, \omega_2) \right]^* \tag{S10}
\end{aligned}$$

Using the above relation we get

$$\begin{aligned}
I_{\beta\alpha}(\omega_2, \omega_1) &= \frac{1}{Z} \sum_{i,f,m} e^{-\beta E_i} \delta(E_i - E_f - \Omega) \left| M_{if}^{\alpha\beta}(\omega_1, \omega_2) \right|^2 \\
&= \frac{1}{Z} \sum_{i,f,m} e^{-\beta E_f} \delta(E_f - E_i - \Omega) \left| M_{fi}^{\alpha\beta}(\omega_1, \omega_2) \right|^2 \\
&= e^{-\beta\Omega} I_{\alpha\beta}(\omega_1, \omega_2). \tag{S11}
\end{aligned}$$

The above relation implies that for $\Omega \rightarrow 0$, the antisymmetric Raman intensity $I_A(\Omega, \theta) \rightarrow 0$.

Reciprocity relation

From the definition of the correlation functions $C_{A_{2g}}^i(t)$, $C_i^{A_{2g}}(t)$ and their Fourier transforms, we have

$$\begin{aligned}
C_{A_{2g}}^i(\Omega) - C_i^{A_{2g}}(\Omega) &= \frac{1}{Z} \sum_{n,m} e^{-\beta E_n} \left[(\hat{\Gamma}_{A_{2g}})_{nm} (\hat{\Gamma}_i)_{mn} \right. \\
&\quad \left. - (\hat{\Gamma}_i)_{nm} (\hat{\Gamma}_{A_{2g}})_{mn} \right] \int_{-\infty}^{\infty} dt e^{i(E_n - E_m + \Omega)t} \\
&= I_{A_{2g}}^i(\Omega) \tag{S12}
\end{aligned}$$

Next, we establish how the correlation functions vary under time reversal operator \hat{K} . The antilinearity of \hat{K} implies the relation

$$\langle n | \hat{A} | n \rangle = \langle \bar{n} | \hat{K} \hat{A} \hat{K}^{-1} | \bar{n} \rangle, \tag{S13}$$

where \hat{A} is any operator and $|\bar{n}\rangle = \hat{K}|n\rangle$. Since a complete set of states $\{|n\rangle\}$ can be replaced by another complete set $\{|\bar{n}\rangle\}$, we have

$$\text{Tr}(\hat{A}) = \text{Tr}(\hat{K} \hat{A} \hat{K}^{-1}). \tag{S14}$$

We consider a system which is intrinsically time reversal symmetric such that the Hamiltonian \hat{H} satisfies $\hat{K} \hat{H}(h) \hat{K}^{-1} = \hat{H}(-h)$, where h is the external magnetic field. In the above equation we set $\hat{A} = e^{-\beta \hat{H}(h)} e^{i \hat{H}(h)t} \hat{\Gamma}_{A_{2g}} e^{-i \hat{H}(h)t} \hat{\Gamma}_i$. This gives

$$\begin{aligned}
C_{A_{2g}}^i(t, h) &= \frac{1}{Z} \text{Tr} \left(e^{-\beta \hat{H}(h)} e^{i \hat{H}(h)t} \hat{\Gamma}_{A_{2g}} e^{-i \hat{H}(h)t} \hat{\Gamma}_i \right) \\
&= -\frac{1}{Z} \text{Tr} \left(\hat{K} \left[\hat{\Gamma}_i e^{i \hat{H}(h)t} \hat{\Gamma}_{A_{2g}} e^{-i \hat{H}(h)t} e^{-\beta \hat{H}(h)} \right] \hat{K}^{-1} \right) \\
&= -\frac{1}{Z} \text{Tr} \left(\hat{\Gamma}_i e^{-i \hat{H}(-h)t} \hat{\Gamma}_{A_{2g}} e^{i \hat{H}(-h)t} e^{-\beta \hat{H}(-h)} \right) \\
&= -\frac{1}{Z} \text{Tr} \left(e^{-\beta \hat{H}(-h)} e^{i \hat{H}(-h)t} \hat{\Gamma}_i e^{-i \hat{H}(-h)t} \hat{\Gamma}_{A_{2g}} \right) \\
&= -C_i^{A_{2g}}(t, -h). \tag{S15}
\end{aligned}$$

In the above we used the fact that the Raman operators are time reversal invariant and that $\hat{\Gamma}_{A_{2g}}$ is antihermitian. Thus, the Fourier transforms satisfy the relation $C_{A_{2g}}^i(\Omega, h) = -C_i^{A_{2g}}(\Omega, -h)$, from which Eq. (7) of the main text follows.

Example (1), antisymmetric response from electronic continuum

We start from the single layer, two orbital model described in example (1) of the main text. Writing $\mathcal{H}_0 = \sum_{\mathbf{k}} \hat{h}_{\mathbf{k}}$, the velocity operators are defined by $\hat{v}_\nu \equiv \sum_{\mathbf{k}} \partial \hat{h}_{\mathbf{k}} / \partial k_\nu$ with $\nu = (x, y)$. This leads to

$$\hat{\Gamma}_{A_{2g}} = \frac{2tV_0}{\bar{\omega}} \sum_{\mathbf{k}} q_{\mathbf{k}} \left(c_{\mathbf{k},x}^\dagger c_{\mathbf{k},y} - \text{h.c.} \right), \tag{S16}$$

$q_{\mathbf{k}} \equiv \epsilon_m / V_0 \sin k_x \sin k_y (\cos k_x + \cos k_y) + \sin^2 k_x \cos k_y + \cos k_x \sin^2 k_y$. Likewise, computing $\partial^2 \hat{h}_{\mathbf{k}} / \partial k_x^2 - \partial^2 \hat{h}_{\mathbf{k}} / \partial k_y^2$ we get

$$\hat{\Gamma}_{B_{1g}} = 2t \sum_{\mathbf{k}} \left(\cos k_x c_{\mathbf{k},x}^\dagger c_{\mathbf{k},x} - \cos k_y c_{\mathbf{k},y}^\dagger c_{\mathbf{k},y} \right). \tag{S17}$$

The next step is to write the above operators in the band basis for which we need the eigensystem of the matrix associated with $\hat{h}_{\mathbf{k}}$. The eigenvalues are

$$\epsilon_{\mathbf{k},a/b} = m_{\mathbf{k}} \pm \sqrt{n_{\mathbf{k}}^2 + V_{\mathbf{k}}^2}, \tag{S18}$$

where $m_{\mathbf{k}} \equiv (\epsilon_{\mathbf{k},x} + \epsilon_{\mathbf{k},y})/2$, $n_{\mathbf{k}} \equiv (\epsilon_{\mathbf{k},x} - \epsilon_{\mathbf{k},y})/2$, $V_{\mathbf{k}}$ is the hybridization, and (a, b) are the band indices. The associated eigenvectors are

$$\begin{pmatrix} u_{\mathbf{k},a} \\ v_{\mathbf{k},a} \end{pmatrix} = \frac{1}{L_{\mathbf{k},a}} \begin{pmatrix} 1 \\ s_{\mathbf{k},a} \end{pmatrix}, \quad \begin{pmatrix} u_{\mathbf{k},b} \\ v_{\mathbf{k},b} \end{pmatrix} = \frac{1}{L_{\mathbf{k},b}} \begin{pmatrix} 1 \\ s_{\mathbf{k},b} \end{pmatrix}, \tag{S19}$$

respectively, where $s_{\mathbf{k},a} = V_{\mathbf{k}} / (\sqrt{n_{\mathbf{k}}^2 + V_{\mathbf{k}}^2} + m_{\mathbf{k}})$, $L_{\mathbf{k},a}^2 = 1 + s_{\mathbf{k},a}^2$, $s_{\mathbf{k},b} = V_{\mathbf{k}} / (\sqrt{n_{\mathbf{k}}^2 + V_{\mathbf{k}}^2} - m_{\mathbf{k}})$, and $L_{\mathbf{k},b}^2 = 1 + s_{\mathbf{k},b}^2$. The antihermitian property of $\hat{\Gamma}_{A_{2g}}$ ensures that it is an interband operator with

$$\hat{\Gamma}_{A_{2g}} = -\frac{2tV_0}{\bar{\omega}} \sum_{\mathbf{k}} q_{\mathbf{k}} \text{Sgn}(V_{\mathbf{k}}) \left(c_{\mathbf{k},a}^\dagger c_{\mathbf{k},b} - \text{h.c.} \right), \tag{S20}$$

where $q_{\mathbf{k}} = (\sin^2 k_x \cos k_y + \cos k_x \sin^2 k_y)$ and Sgn is the sign function. Likewise, for the Hermitian operator $\hat{\Gamma}_{B_{1g}}$ we get

$$\hat{\Gamma}_{B_{1g}} = \frac{t|V_{\mathbf{k}}|}{\sqrt{n_{\mathbf{k}}^2 + V_{\mathbf{k}}^2}} (\cos k_x + \cos k_y) \left(c_{\mathbf{k},a}^\dagger c_{\mathbf{k},b} + \text{h.c.} \right) + \dots, \tag{S21}$$

where the ellipsis imply intraband operators that do not enter the calculation. The evaluation of the cross-susceptibility follows standard steps, and we get

$$\begin{aligned}
\chi_{A_{2g}}^{B_{1g}}(i\Omega_n) &= -\frac{2t^2V_0}{\bar{\omega}} \frac{1}{\Omega_0\beta} \sum_{\mathbf{k}, \omega_n} g_{\mathbf{k}} \\
&\quad \times \{ G_b(\mathbf{k}, i\omega_n + i\Omega_n) G_a(\mathbf{k}, i\omega_n) - a \leftrightarrow b \}. \tag{S22}
\end{aligned}$$

In the above $g_{\mathbf{k}} = (\cos k_x + \cos k_y) V_{\mathbf{k}} q_{\mathbf{k}} / p_{\mathbf{k}}$, with $p_{\mathbf{k}} = ((\epsilon_{\mathbf{k},x} - \epsilon_{\mathbf{k},y})^2 / 4 + V_{\mathbf{k}}^2)^{1/2}$, $G_{a/b}(\mathbf{k}, i\omega_n) = 1 / (i\omega_n - \epsilon_{\mathbf{k},a/b})$. From the above we also have $\chi_{A_{2g}}^{B_{1g}}(-i\Omega_n) = -\chi_{A_{2g}}^{B_{1g}}(i\Omega_n)$, which implies that $\phi_{A_{2g}}^{B_{1g}}(i\Omega_n) = 2\chi_{A_{2g}}^{B_{1g}}(i\Omega_n)$.

If we assume the electronic excitations to be undamped, the frequency sum can be performed analytically. We get

$$L_{ab}(\mathbf{k}, i\Omega_n) \equiv \frac{1}{\beta} \sum_{\omega_n} G_a(\mathbf{k}, i\omega_n) G_b(\mathbf{k}, i\omega_n + i\Omega_n)$$

$$= \frac{n_F(\epsilon_{\mathbf{k},a}) - n_F(\epsilon_{\mathbf{k},b})}{i\Omega_n + \epsilon_{\mathbf{k},a} - \epsilon_{\mathbf{k},b}}, \quad (\text{S23})$$

where n_F is the Fermi function. This gives,

$$\begin{aligned} \phi_{A_{2g}}^{B_{1g}}(i\Omega_n) &= -\frac{4t^2 V_0}{\bar{\omega}} \frac{1}{\Omega_0} \sum_{\mathbf{k}} g_{\mathbf{k}} (n_F(\epsilon_{\mathbf{k},a}) - n_F(\epsilon_{\mathbf{k},b})) \\ &\times \left\{ \frac{1}{i\Omega_n + \epsilon_{\mathbf{k},a} - \epsilon_{\mathbf{k},b}} + \frac{1}{i\Omega_n + \epsilon_{\mathbf{k},b} - \epsilon_{\mathbf{k},a}} \right\}. \end{aligned}$$

The other limit where the frequency sum can be performed analytically is with finite electron lifetime but at $T = 0$. In this limit

$$\begin{aligned} L_{ab}(\mathbf{k}, \Omega + i\eta) &= \frac{1}{2\pi i} \left[\frac{J_1(\mathbf{k}, \omega)}{\Omega + \epsilon_{\mathbf{k},a} - \epsilon_{\mathbf{k},b}} \right. \\ &\left. + \frac{J_2(\mathbf{k}, \omega)}{\Omega + 2i\gamma + \epsilon_{\mathbf{k},a} - \epsilon_{\mathbf{k},b}} \right], \quad (\text{S24}) \end{aligned}$$

where

$$\begin{aligned} J_1(\mathbf{k}, \omega) &= \ln(\Omega - \epsilon_{\mathbf{k},b} + i\gamma) + \ln(-\Omega - \epsilon_{\mathbf{k},a} - i\gamma) \\ &- \ln(-\epsilon_{\mathbf{k},a} + i\gamma) - \ln(-\epsilon_{\mathbf{k},b} - i\gamma), \quad (\text{S25}) \end{aligned}$$

$$\begin{aligned} J_2(\mathbf{k}, \omega) &= -\ln(\Omega - \epsilon_{\mathbf{k},b} + i\gamma) - \ln(-\Omega - \epsilon_{\mathbf{k},a} - i\gamma) \\ &+ \ln(-\epsilon_{\mathbf{k},a} - i\gamma) + \ln(-\epsilon_{\mathbf{k},b} + i\gamma). \quad (\text{S26}) \end{aligned}$$

The computations for example (1) were performed using this limit.

For the numerical evaluation we set $t_1 = 2$ eV, $t_2 = 0.37$ eV, $\mu = 1.5$ eV, $V_0 = 0.32$ eV and $\epsilon_m = 0.35$ eV. The resulting Fermi surface is shown in Fig. 2(a) of the main text. The threshold for interband transitions is given by $\Omega_{ph} = 2V_0$ in the $\gamma \simeq 0$ limit, while it develops a tail at lower frequencies when the electron broadening is increased. In Fig. 1(c)-(d) of the main text we set $\gamma = 0.05$ eV.

Example (2), amplitude mode of the CDW phase

Starting from the two-orbital model discussed in example (1), the CDW phase can be effectively described by adding the mean-field inter-orbital interaction $\mathcal{H}_{int} = \Delta \sum_{\mathbf{k}} [c_{\mathbf{k}+\mathbf{Q},x}^\dagger c_{\mathbf{k}-\mathbf{Q},y} + c_{\mathbf{k}+\mathbf{Q},y}^\dagger c_{\mathbf{k}-\mathbf{Q},x} + \text{h.c.}]$ to the total Hamiltonian $\mathcal{H} = \mathcal{H}_0 + \mathcal{H}_{int}$. The amplitude mode is associated with amplitude fluctuations of the CDW order parameter Δ around its equilibrium position. Its contribution to the Raman response is obtained as the vertex correction in the amplitude channel of the bare electronic response, which corresponds, from a diagrammatic perspective, to the two-loop contribution shown in Fig. 1(b) of the main text. The two fermionic susceptibilities in Eq.(8) of the main text explicitly read

$$\begin{aligned} \chi_{A_{2g}}^{\Delta}(i\Omega_n) &= \frac{1}{\Omega_0 \beta} \sum_{\mathbf{k}, \omega_n} \text{Tr} \left[\hat{\Gamma}_{A_{2g}} \hat{G}(\mathbf{k}, i\omega_n + i\Omega_n) \hat{\Delta} \hat{G}(\mathbf{k}, i\omega_n) \right], \\ \chi_{\Delta}^i(i\Omega_n) &= \frac{1}{\Omega_0 \beta} \sum_{\mathbf{k}, \omega_n} \text{Tr} \left[\hat{\Delta} \hat{G}(\mathbf{k}, i\omega_n + i\Omega_n) \hat{\Gamma}_i \hat{G}(\mathbf{k}, i\omega_n) \right], \quad (\text{S27}) \end{aligned}$$

where $i = (B_{1g}, B_{2g})$, $\hat{\Delta} \equiv \partial \hat{\mathcal{H}}_{int} / \partial \Delta$ is the scattering vertex due to the amplitude mode and $\hat{G}(\mathbf{k}, i\omega) = (i\omega - \hat{\mathcal{H}}_{\mathbf{k}})^{-1}$ is the electronic Green's function, with $\hat{\mathcal{H}}_{\mathbf{k}}$ written in the extended orbital basis defined by the $\Psi_{\mathbf{k}} = (c_{\mathbf{k}-\mathbf{Q},x}, c_{\mathbf{k}+\mathbf{Q},x}, c_{\mathbf{k}-\mathbf{Q},y}, c_{\mathbf{k}+\mathbf{Q},y})^T$ spinor, such that $\mathcal{H} = \sum_{\mathbf{k}} \Psi_{\mathbf{k}}^\dagger \hat{\mathcal{H}}_{\mathbf{k}} \Psi_{\mathbf{k}}$. Following the same procedure detailed in the previous Section, it is convenient to write \hat{G} in the band basis and perform the frequency sum at $T = 0$. One then introduces a finite electron lifetime γ , set to $\gamma = 0.1\Delta$ with $\Delta = 0.1$ eV in Fig. 2 of the main text. The tight-binding parameters are the same detailed in example (1), while the ordering wave-vector is set to $\mathbf{Q} = \sqrt{2}Q_0 \{\cos[(1+r)\pi/4], \sin[(1+r)\pi/4]\}$, with $Q_0 = 5\pi/8$. The amplitude mode propagator is well described by a Lorentzian function $D(\Omega) = 2E_0 / [(\Omega + i\gamma_0)^2 - E_0^2]$, with $E_0 = 0.005$ eV and $\gamma_0 = 0.2E_0$.